▌ **Polyoxometalates** | *Hot Paper* |

Polyoxometalate/Polyethylene Glycol Interactions in Water: From Nanoassemblies in Water to Crystal Formation by Electrostatic Screening

Thomas Buchecker,[a, b] Xavier Le Goff,[b] Bappaditya Naskar,[c] Arno Pfitzner,[a] Olivier Diat,[b] and Pierre Bauduin*[b]

Abstract: In the last decade organic–inorganic hybrid materials have become essential in materials science as they combine properties of both building blocks. Nowadays the main routes for their synthesis involve electrostatic coupling, covalent grafting, and/or solvent effects. In this field, polyoxometalates (POMs) have emerged as interesting inorganic functional building blocks due to their outstanding properties. In the present work the well-known α-Keggin polyoxometalate, α-$PW_{12}O_{40}^{3-}$ (PW), is shown to form hybrid crystalline materials with industrial (neutral) polyethylene glycol oligomers (PEG) under mild conditions, that is, in aqueous medium and at room temperature. The formation of these materials originates from the spontaneous self-assembly of PW with EO_x, (EO=ethylene oxide) with at least four EO units ($x > 4$). The PW–PEG nanoassemblies, made of a POM surrounded by about two PEG oligomers, are stabilized by electrostatic repulsions between the negatively charged PW anions. Addition of NaCl, aimed at screening the inter-nano-assembly repulsions, induces aggregation and formation of hybrid crystalline materials. Single-crystal analysis showed a high selectivity of PW towards EO_5–EO_6 oligomers from PEG200, which is made of a mixture of EO_{3-8}. Therefore, a general "soft" route to produce POM–organic composites is proposed here through the control of electrostatic repulsions between spontaneously formed nanoassemblies in water. However, this rational design of new POM hybrid (crystalline) materials with hydrophilic blocks, using such a simple mixing procedure of the components, requires a deep understanding of the molecular interactions.

Introduction

Polyoxometalates (POMs) are anionic metal-oxygen clusters consisting of oxo-linked MO_x polyhedra of early transition metals in their highest oxidation state.[1] Their electronic versatility and the blend of *p*-block elements, transition metals, and differently bound oxygen atoms (terminal and bridging) grant special properties resulting in a broad field for applications such as catalysis,[2,3] material science,[4,5] biology,[6,7] and medicine.[8–10] For most of these applications the understanding of the interactions between inorganic POM clusters and organic entities is essential.

In this context, much effort has been made in the design and building of POM–organic hybrid assemblies. Many examples of such hybrid POM systems are provided in recent comprehensive reviews, for example, by Proust et al.[11] and Cronin et al.[12] The design of POM–organic composite materials is mostly based on two approaches: an electrostatic coupling between an anionic POM with an organic cation and a covalent coupling with the POMs chemically grafted to organic moieties. POMs fixed at electrodes,[13] embedded in polymers,[14] and organized in an hierarchical self-assembly[15–22] are examples that meet the former case. In a recent contribution of Izzet et al., hierarchical self-assembly of POM hybrids has been achieved by using an approach that combines electrostatic interactions and metal coordination of a POM chemically-grafted building block.[18] Interestingly, the self-assembly process in this latter system, from discrete assemblies to nanoaggregates, was tuned by changing the type of solvent. On the other hand, covalent grafting has been used to immobilize POMs on surfaces or interfaces,[23] in mesoporous materials,[24,25] and in the synthesis of POM based surfactants to form either microemulsion systems[26] or smart electrochemically responsive materials.[27]

Recently, the strong propensity of the α-Keggin based POMs, silico- and phospho-tungstate (α-$SiW_{12}O_{40}^{4-}$ and α-

[a] M. Sc. T. Buchecker, Prof. Dr. A. Pfitzner
Institute of Inorganic Chemistry
University of Regensburg
93040 Regensburg (Germany)

[b] M. Sc. T. Buchecker, Dr. X. Le Goff, Dr. O. Diat, Dr. P. Bauduin
Institut de Chimie Séparative de Marcoule (ICSM)
UMR 5257 (CEA, CNRS, UM, ENSCM), BP 17171
30207 Bagnols-sur-Cèze (France)
E-mail: pierre.bauduin@cea.fr

[c] Dr. B. Naskar
Department of Chemistry
Sundarban Hazi Desarat College
University of Calcutta
Pathankhali, 743611 (India)

⬚ Supporting information for this article can be found under:
http://dx.doi.org/10.1002/chem.201700044.

$PW_{12}O_{40}{}^{3-}$), to adsorb on neutral soft interfaces covered with polar organic moieties, such as sugar and ethylene oxide (EO) groups, was highlighted.[28] POMs were indeed shown to adsorb at the micellar surface of, for example, tetraethyleneglycol mono-octyl ether (C_8EO_4) and octyl beta-glucoside (C_8G_1), without disrupting the micellar assembly. It was also shown that the adsorption of POMs is not restricted to the micelle-water interface but it also takes place at the water-air surface covered by these two surfactants. These findings give an opportunity for the formation of hybrid POM materials by another approach that is based on neither pure electrostatic or covalent grafting but that takes advantages of weak intermolecular forces between POMs and polar organic functional groups in aqueous solution.

Consequently, the aim of this work was: (i) to study more specifically the POM–(poly-)ethylene glycol (PEG) supramolecular interactions previously observed at the micelle-water and water-air interface and (ii) to investigate the potential of using POM–PEG interactions to build up highly ordered hybrid POM-based materials. This work is restricted to the investigation of weak interactions, that is, neither electrostatic nor covalent bonds, acting between POM and polar organic functional groups. These interactions were probed in the most green solvent, that is, water, without using the polar organic solvents classically used in POM chemistry, such as acetonitrile or DMSO.

The strategy applied here was to simplify the chemical systems by investigating the interactions in water between the POM, α-$PW_{12}O_{40}{}^{3-}$ (PW, see Figure 1a), and the polar head of PEG based non-ionic surfactants, that is, simple oligomeric PEG chains (Figure 1b and c). Therefore, only the POM–PEG interactions without surface effects were probed in the present contribution. POMs and PEG chains are not expected to interact in water as they are anionic and electrically neutral, respectively, and also as they are both highly hydrophilic/water-soluble.

PEGs have an outstanding importance in medicine as well as in chemistry, biology, and industry due to their low price and high biocompatibility.[29, 30] They are widely applied in product and drug formulations, chemical reactions, and in advanced functional materials.[31–34] Hence, composite materials of POM and EO_x oligomers may become important as the combination of both the catalytic performance of POMs and above mentioned benefits of PEG could lead to advantageous materials with superior performances. Therefore, lots of work has already been performed on this subject.[35–39] In 1989, Neumann et al. observed an elevated catalytic activity of POMs in the presence of PEG.[39] In materials science, layered PEG–POM structures consisting of PEG chains covalently grafted to a POM, have been constructed.[36,37] Only recently, non-covalently bound POM–PEG composites were produced through a hydrothermal route and characterized as intermediate temperature proton conductors.[38]

In the present work, PEG–PW interactions were probed in water at room temperature and at low concentrations ($<$ 100 mM), much below the solubility limits of the components, by varying the chain length of PEG for a series of compounds from pure EO_1 to EO_4. Longer EO_x were tested as well but as they are difficult to obtain with a pure grade, industrial mixtures were used: PEG200 (equivalent in average to EO_4), PEG300 ($\approx EO_6$), PEG400 ($\approx EO_8$), and PEG20000 ($\approx EO_{400}$). Industrial grade PEG_x show dispersity in their chain lengths, that is, in their number of EO units. PEG200 for example covers a range EO_x from $x = 3$ to 8 with a majority (around 90%) being EO_4, EO_5, and EO_6, as analyzed by mass spectroscopy (see Supporting Information).

PW–EO_x interactions were studied by combining several techniques with different focus. Small angle X-ray scattering (SAXS) experiments were performed as a function of POM/EO_x ratios to obtain information on electron density inhomogeneity coming mainly from the POM and the surrounding medium composed of water and EO_x. Small angle neutron scattering (SANS) measurements were performed in deuterated water in order to gain structural and supramolecular information on the hydrogenated EO_x oligomers. Furthermore, ^{1}H-NMR was used to yield information at a molecular level on the chemical environment of the hydrogen atoms of EO_x in the presence of POM.

Since from a previous investigation the addition of excess salt is known to screen electrostatic interactions between negatively charged POM anions,[28] the impact of salt addition on the EO_x–POM mixtures was also investigated. The formation of a solid phase and the formation of crystals consisting of EO_x–PW composites were investigated by SAXS as well as by single-crystal XRD. An attempt was made here to correlate interactions taking place between POM and EO_x in aqueous solution with the highly ordered structure obtained in the solid state.
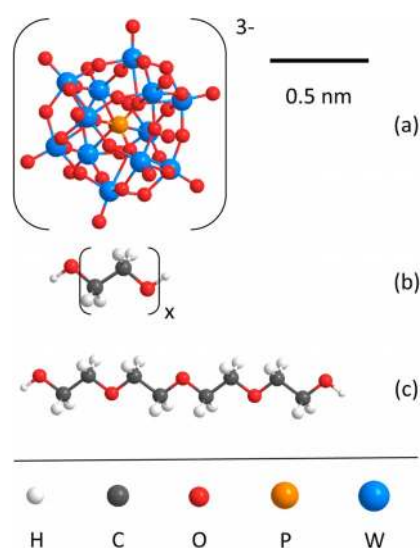

Figure 1. Optimized structures of (a) α-$H_3PW_{12}O_{40}$ (PW), (b) the EO_x oligomer repeating unit, and (c) the main component in PEG200, that is, EO_4. PW–EO_x interactions were investigated as a function of its ratio, EO_x chain length and EO_x concentration. Polydisperse PEG chemicals (PEG200, PEG300, PEG400, and PEG20000) were used to cover a broad range of EO_x oligomer chain lengths.

Results and Discussion

A concentration of 50 mm EO_1–EO_4 and PEG (200, 300, 400, 20000) in an aqueous media of HPW, the acidic form of PW, provides clear isotropic solutions at any proportions without the formation of any precipitate visible at the macroscopic level.

PW–EO_x nanoassemblies by small angle X-ray scattering (SAXS)

The SAXS spectra of 25 mm PW in pure water and in the presence of 50 and 100 mm PEG200 are depicted in Figure 2a. All spectra overlap in the high q-regime ($q > 5$ nm^{-1}) where the scattered intensity comes mainly from the POM, that is, its form factor and its concentration. At low q values ($q < 0.5$ nm^{-1}) where inter-molecular/sub-molecular distances are concerned, all spectra show a decreased intensity indicating strong repulsive interactions between negatively charged POMs.[28] The spectra of PEG–PW show excess scattering in the low q-range ($q < 4$ nm^{-1}) compared to the pure PW spectrum. The excess scattering increases and shows a maximum value that is shifting to lower q values, that is, larger distances, with increasing PEG200 concentration. These two last features observed in the spectra by adding PEG200 can be attributed to an excess of electron density (compared to water) around the POM and to the formation of a structure larger than the POM alone (≈ 1 nm in size), respectively. Therefore, the SAXS spectra can be interpreted by the formation of POM–PEG self-assemblies, with the POM decorated by PEG oligomers, which have an electron density higher than the one of water.

The SAXS spectra for such nanoassembled structures were simulated and compared to the experimental spectra. PW–$(EO_4)_x$ nanoassemblies with different molecular arrangements and x values were designed in silico and their SAXS spectra were calculated from their spatial atomic positions by using the CRYSOL software.[40] Snapshots of the different molecular

arrangements, the simulated curves, and the details of the procedure to produce the simulated spectra are given in the Supporting Information. The simulated spectra for PW and for PW–EO_4 nanoassemblies with 1:2 and 1:4 ratios, that is, PW-2(EO_4) and PW-4(EO_4), (see solid lines in Figure 2) have shapes similar to the experimental spectra obtained for PW–PEG200 at different PEG concentrations. Both the shift to lower q values and the increase in the excess scattered intensity is reproduced in the simulations. The consistency between the experimental and simulated spectra suggests that PEG oligomers bind with PW in water and that PWs are getting more and more surrounded by PEG oligomers with increasing PEG/PW ratio.

In a previous investigation, Keggin POMs were found to adsorb on the surface of micelles of non-ionic PEG/sugar based surfactants.[28] In order to ensure that such a structure, formed by PEG(s) surrounded by POMs, does not form in PEG/PW mixtures, simulations of PW–PEG_x nanoassemblies made of a core of many PEG_x oligomer(s) surrounded with PWs, were investigated (see Figure S1 in Supporting Information). Such hypothetical molecular arrangements give SAXS spectra with a strong oscillation in the mid q-range, at around 2 nm^{-1}, originating from strong POM–POM repulsions. Such an oscillation was never observed in the experimental spectra confirming that PW–PEG assemblies consist of single POMs decorated with PEG oligomers.

In order to get a deeper understanding of PW–PEG interactions in water, EO_1–EO_4 and PEG300/PEG400/PEG20000 were also investigated by SAXS in the presence of PW (see Figure S2 in Supporting Information). Scattering spectra of EO_1–EO_4/PW mixtures overlap the spectrum of pure PW in water over the whole q-range, suggesting that no assembly is formed. The spectra of PEG300/PEG400/PEG20000–PW clearly show excess scattering in the low q-range ($q < 4$ nm^{-1}) compared to the PW spectrum; the same holds for PEG200. By increasing the length of PEG, the excess scattering and the maximum in the scattered intensity, respectively, become more pronounced and are shifted to lower q values. Considering that electrostatic repul-
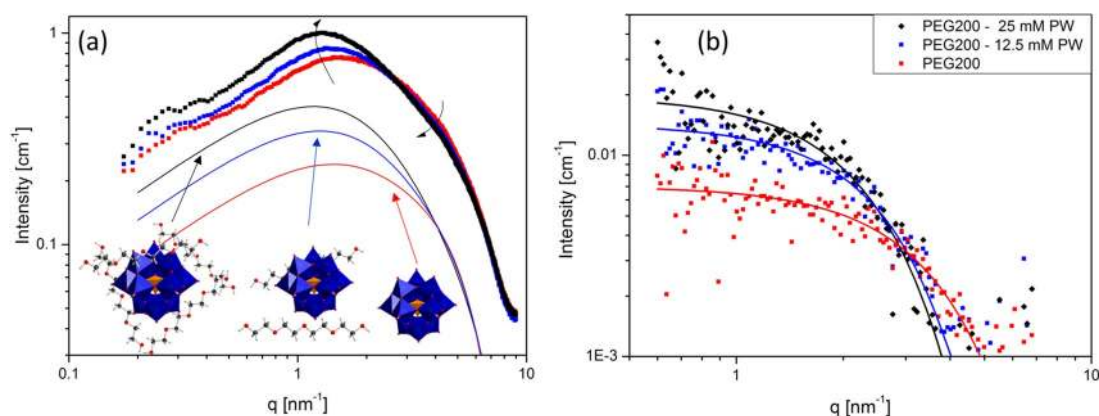

Figure 2. The interaction of EO_x/PEG–POM monitored on a molecular level. (a) SAXS spectra of 0 mm (red), 50 mm (blue), and 100 mm PEG200 (black) in the presence of 25 mm PW. The scattering pattern of PEG200 in water is not shown as c(PEG200) < 100 mm does not produce a detectable signal compared to the spectrum of pure water. Theoretical simulations (solid lines) of SAXS spectra for hypothetical molecular arrangements of PW–PEG assemblies: PW alone (red), PW with two EO_4 oligomers in fully extended conformation, PW–2(EO_4), (blue), and PW with four EO_4 oligomers, PW–4(EO_4), in fully extended conformation (black). For the sake of clarity, the simulated spectra are shifted in intensity from the experimental spectra. (b) SANS spectra of 50 mm PEG200 as representative model for EO oligomers in the presence of 0, 12.5, and 25 mm PW.

sions between the aggregates take place, the size of the PW–EO_x assemblies cannot be estimated by applying a Guinier analysis. As a rough estimation, the intensity decrease in the q-range $1 < q < 3$ nm^{-1} indicates that aggregates with an average radius from 0.6 to 1 nm are formed. Comparing these average radii to the hydrodynamic radii of pure PW in water, that is, 0.5 nm (see Figure S3), also confirms the presence of nanoassemblies of PW–PEG. Moreover, this scattering signal is shifted to smaller q values from PEG300 to PEG400 to PEG20000 indicating that larger nanoassemblies are formed with increasing EO_x chain lengths. The comparison of the experimental and simulated spectra (see Figure S1), indicates that PEG300–PW and PEG400–PW assemblies produce similar scattering patterns to those of PW surrounded by 3 and 7 EO_4 oligomers, respectively. Therefore, it can be concluded that the extent of excess scattering and the shift of the q_{max} values depend on the absolute number of EO_x oligomers around PW. The change in the conformation of the EO_4 oligomer, from an extended to a U-shaped conformation, alters only slightly the simulated SAXS scattering pattern of EO_x decorated PW assemblies. Therefore, no configurational information can be derived from SAXS.

From these scattering experiments we can deduce that the formation of PW–EO_x assemblies is promoted and reinforced by longer EO_x oligomers $x \geq 4$ and that the size of these assemblies increases with the length of the EO_x oligomer, once a critical EO_x chain length is reached, that is, for $x > 4$.

PW–EO_x nanoassemblies by small angle neutron scattering (SANS)

SAXS gives a first proof of the PW/EO_x interactions taking place in water and leading to their self-assembly. The scattering contrast in SAXS originates here from inter and intra correlation of the POM which has a very high electron density due to the presence of tungsten atoms. In order to investigate further the PW–EO_x self-assembly, SANS experiments were performed on PEG200/PW mixtures in D_2O. The advantage of performing SANS in the present system is that PW produces almost no contrast with D_2O and a constant scattered intensity is observed over the whole q-range. For the sake of clarity this spectrum is not shown in Figure 2b. Therefore, only the hydrogenated PEG200 contributes to the coherent scattered intensity. Figure 2b shows the SANS spectra of PEG200 at 50 mM in D_2O for different PW concentrations: 0, 12.5, and 25 mM, corresponding to PEG/PW molar ratios of 1/0, 4/1, and 2/1. The spectrum of 50 mM PEG200 shows the typical scattering of globular objects. Addition of PW leads to an increase in the forward scattering, $I(0)$, and to a slight shift of the scattering spectra towards lower q, which indicates the formation of larger scattering objects. However, the difference between the spectra at 12.5 and 25 mM remains weak.

A Guinier model, $I(q) = I(0)exp^{(-q^2 R_g/3)}$, was applied and showed an increase in the mean radii of gyration (R_g) of the aggregates from 0.5 (0 mM PW), 0.7 (12.5 mM PW) to 0.8 nm (25 mM PW), confirming the increasing size of the scattering object when adding PW. The estimation of the radius here is however questionable as inter-particles interactions take place,

especially at 25 mM PW. The $I(0)$ values were analyzed by assuming the scattering of isotopically distributed objects in Equation (1):

$$I(0) = nV^2(\Delta\rho)^2 \tag{1}$$

with n being the concentration of the scattering objects, V their volume, and $\Delta\rho$ the scattering length density difference between D_2O and the scattering objects. By assuming that PEG200 oligomers only contribute to the scattered signal in SANS and that PEG200 is mostly composed of EO_4, then the forward scattered intensity can be rewritten as Equation (2):

$$I(0) = [PEO_4]N_{agg}V_{EO_4}^2(|\rho_{D_2O} - \rho_{PEO_4}|)^2 \tag{2}$$

with [EO_4] the PEG200 concentration, N_{agg} the number of EO_4 in EO_x–PW assemblies, $V_{EO_4}^2$ the molecular volume of EO_4, and ρ the scattering length densities of D_2O and EO_4. The experimental spectra were fitted by adjusting only N_{agg} as the other parameters are known. The N_{agg} values obtained by this approach are 1.0, 2.0, and 2.2 for 0, 12.5, and 25 mM PW and correspond to averaged aggregation numbers with an error estimated to be at least 0.5 as inter-particle interactions take place. Only averaged N_{agg} values can be estimated as the PEG can be present in solution as a mixture of unassociated oligomers and PW associated oligomers (PW–EO_4, PW–2(EO_4), PW–3(EO_4) etc.). From the SANS results it can be concluded that PEG200 is in monomeric form, that is, non-aggregated at 50 mM in pure water and that addition of PW leads to PEG200 aggregation. By combining the SAXS/SANS results, it can be stated that PW–PEG200 nanoassemblies consist of a POM surrounded by an average of two PEG oligomers.

Molecular interactions in the nanoassemblies probed by NMR

^{1}H-NMR was performed to probe the change in the local environment of the PEG_x oligomers caused by their adsorption on PW. Previous studies have shown that NMR is an efficient technique to probe molecular interactions of PEG with, for example, zeolites[41] or proteins.[42]

PEG200 was chosen as an EO_x representative as SAXS and SANS experiments clearly showed the presence of PW–PEG200 nanoassemblies. Hence, ^{1}H-NMR spectra of 100 mM PEG200 solutions in D_2O were collected for different PW concentrations (0, 20, 50, 100 mM) as shown in Figure 3. The spectrum for 0 mM PW depicts three resonance signals: a multiplet from 3.55 to 3.62 ppm, a multiplet from 3.65 to 3.70 ppm and a sharp singlet at 3.65 ppm (marked with *). By considering EO_4 ($C_8O_5H_{18}$), the main component of PEG200, hydrogen atoms can be assigned by using Shoolery's rules for the NMR increment of -CH_2- groups.[43] The multiplet overlapping with the large singlet at 3.65 to 3.70 ppm is assigned to the -CH_2-CH_2-OH (brown). The large singlet is assigned to the magnetically equivalent inner -O-CH_2-CH_2-O- groups (blue)[41,44] and the multiplet from 3.55 to 3.62 ppm is assigned to the CH_2 groups connected to the terminal -CH_2OH groups -CH_2-CH_2-OH (black).
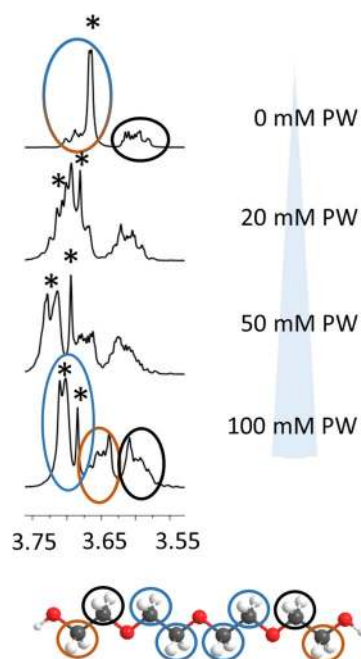
Figure 3. NMR resonance signals of 100 mм PEG200 in the presence of 0, 25, 50, and 100 mм PW (from top to bottom) and qualitative assignment of the protons of the main component of PEG200, that is, EO_4, to the resonance signals. The stars indicate the change in intensity of the resonance signal stemming from the inner protons (blue circles) and the emergence of a doublet of PEG200, which represents PEG200 adsorbed on PW.
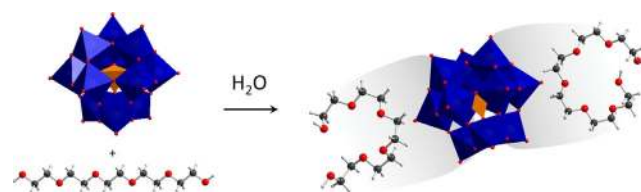

Figure 4. Schematic representation of the PW–PEG nanoassemblies in aqueous solution. Scattering methods (SAXS, SANS) and NMR spectra revealed an accumulation of roughly two PEG oligomers in a loop shape configuration around one PW anion. The SAXS/SANS combination provides information on the structure of supramolecular assemblies, that is, a POM surrounded by PEG oligomers, and NMR spectroscopy informs on the special interaction of the inner -CH_2-groups of PEG with PW supporting the loop shape model of PEG in PW–PEG nanoassemblies.

The O—H protons of the terminal hydroxyl groups are not visible in this NMR setup due to their fast intermolecular exchange with the solvent.[45]

Addition of PW to PEG200 produces two main effects on the spectra: a shift of the large singlet to the deep-field and an intensity decrease of the singlet and the emergence of a doublet which increases in intensity with increasing PW concentration (marked with *). This last trend as a function of PW concentration indicates that the singlet and the emerging doublet correspond, respectively, to the unassociated and associated form of the PEG in solution. Therefore, the progressive formation of the nanoassemblies by increasing PW concentration is monitored. For 100 mм PW the three signals are well separated and can therefore be integrated separately giving a hydrogen ratio of 8:4:4. A detailed integration of the multiplets is shown in Figure S4 (Supporting Information). The multiplet at 3.57 ppm can still be attributed to the terminal -CH_2- groups (red) as it remains almost constant with increasing PW concentration. The multiplet initially at 3.67 ppm also remains almost constant. Only the singlet corresponding to the inner hydrogen atoms of EO_4 shifts to deep-field upon addition of PW. Therefore, NMR suggests that the hydrogen atoms of the two inner EO units strongly interact with PW whereas CH_2 groups in the two terminal EO moieties do not take part in the self-assembly between PW and EO_x oligomers (Figure 4). Note that, for NMR experiments, higher PW concentrations were chosen compared to SAXS/SANS experiments in order to highlight the trend of the splitting and shifting of the resonance signals. Furthermore, additional NMR experiments on the pure EO_4 com-

pound, that is, tetraethylene glycol, were performed to obtain further information on the adsorption process for shorter chain EO_x oligomers (Figure S5). Indeed, a shift of an intense singlet to the deep-field was observed (as it was the case for PEG200). However, no splitting of the singlet and no changes in the relative intensities of the resonance signals were observed. Furthermore, the relative chemical shift, $\delta\ \Delta$ppm, upon addition of PW, is smaller compared to the relative chemical shift of PEG200 upon PW addition. Therefore, it can be concluded that pure EO_4 also interacts with PW, but only at higher concentrations of PW in comparison to PEG200.

In order to prove that the shift of the singlet and the emergence of the doublet do not originate from a classical salt effect or from the acidic protons of PW, NMR spectra of PEG200 were collected in the presence of various salts and with similar acidity using HCl. These tests did not result in significant changes of the shape and the shift of the resonance peaks (Figure S6 and S7). Consequently, the changes observed in the ^{1}H-NMR spectra by increasing PW concentration can be attributed to the formation of PW–PEG_x nanoassemblies in water. It should be noted that the NMR signal of PEG200 is interpreted as coming from its main component, that is, EO_4, because the integration of the three ^{1}H-NMR signals gave the ratio 8/4/4 for H atoms of inner and outer EO moieties. This assumption is however validated by the average number of EO unit in PEG200 which is generally considered to be 4, as deduced from its average molar mass. The complexity of the NMR spectra showing many overlapping peaks may arise from the polydispersity of PEG200 which is composed of a mixture of EO_x oligomers with x ranging from 3–8 as measured by electro-spray ionization-mass spectroscopy (see Figure S8). From the qualitative assignment of NMR resonance signals of the PEG200 compound, it can be concluded that PW interacts with EO_x oligomers and that PW additionally interacts preferentially with the inner protons of the EO_x oligomer, as shown in the sketch of the nanoassembly in Figure 4.

From nanoassemblies in water to crystal formation by screening of electrostatic repulsions

In a previous study it was shown by SAXS that addition of salts, such as NaCl, to POM aqueous solutions leads to the

screening of electrostatic repulsions between the POM anions.[28] A salt induced screening effect was also previously observed between non-ionic micelles decorated by POMs.[28] In the following, the screening of electrostatic repulsions in the PW–(EO)$_x$ mixtures was investigated for a fixed PW concentration of 25 mM by adding 100 mM NaCl, which is sufficient to screen most of the electrostatic repulsions.

In the case of EO$_1$, EO$_2$, EO$_3$, and EO$_4$, the solutions stayed clear in the presence of NaCl in the concentration range of [EO$_x$] from 5 to 500 mM and no changes in the SAXS spectra were observed compared to the spectrum of pure PW (25 mM) with NaCl (100 mM, Figure S9). On the contrary for PEG200, PEG300, and PEG400, white crystalline precipitates were formed instantly after mixing PEG–NaCl and PW–NaCl solutions. For the much longer EO$_x$ oligomers, that is, PEG20000, the solution became cloudy after mixing with PW/NaCl and streak-like or coacervate-like structures, were formed (see the optical microscope images in Figure S10). Consequently, precipitation only takes place when PW–PEG nanoassemblies are present in solution suggesting that the precipitates originate from the aggregation of the nanoassemblies caused by a screening of electrostatic repulsions between them. To gain further insight into the structure of the PEG (200, 300, 400)–PW composite materials, crystal growth conditions have been optimized to obtain large crystals suitable for single-crystal analysis. The experiments focused on the concentration variation of PEG (200, 300, 400) from 12.5 up to 100 mM. The concentration of PW was varied between 25 and 50 mM and the concentration of NaCl was kept constant at 100 mM. It has to be mentioned that the PW concentration was much below its solubility limit in water (> 900 mM). As a general trend, crystal size decreases with increasing PEGx concentration and with increasing x. For PEG200, millimeter size crystals with a hexagonal habit were obtained. These crystals were sufficiently large to be investigated by single-crystal X-ray diffraction. The largest crystals were obtained by using 50 mM PEG200, 50 mM PW, and 100 mM NaCl (see microscopy images in Figure S11 and S12).

The single-crystal analysis reveals a monoclinic crystal system and a primitive lattice, space group $P2_1/c$, with the parameters given in Table S1 in the Supporting Information. The asymmetric unit of the unit cell consists of one PW anion and three sodium cations entangled by two EO$_x$ oligomer chains (one EO$_5$ and one EO$_6$) as shown in Figure 5. Sodium cations counterbalance the charge of the PW anion, and almost all oxygens of polydentate EO$_x$ oligomers coordinate to Na$^+$ (Figure 5 and Figure 6). Four water molecules per asymmetric unit are incorporated into the crystal structure. The latter also coordinate towards Na$^+$ and link two of the three Na$^+$ cations. Further information on the parameters of the single-crystal structure analysis can be found in Table S1 and an IR characterization of the compound can be seen in Figure S13.

A powder diffraction pattern was calculated from the single crystal data and was compared to an experimental pattern of the precipitate obtained by using 50 mM PEG200, 25 mM PW, and 100 mM NaCl. Both diffractograms coincide almost perfectly in most of the reflections indicating that the structure
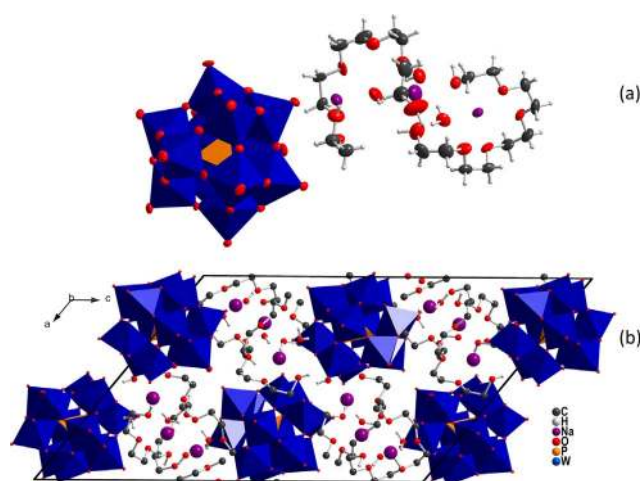

Figure 5. (a) Asymmetric unit of the structure model of $C_{22}H_{56}Na_3O_{57}PW_{12}$ represented with displacement ellipsoids (probability factor 70%). Split positions are not shown in this representation. (b) Packing of the elementary cell projected along [0 1 0]. For the sake of clarity, atoms are not displayed with displacement ellipsoids and hydrogen atoms connected to carbon are omitted.
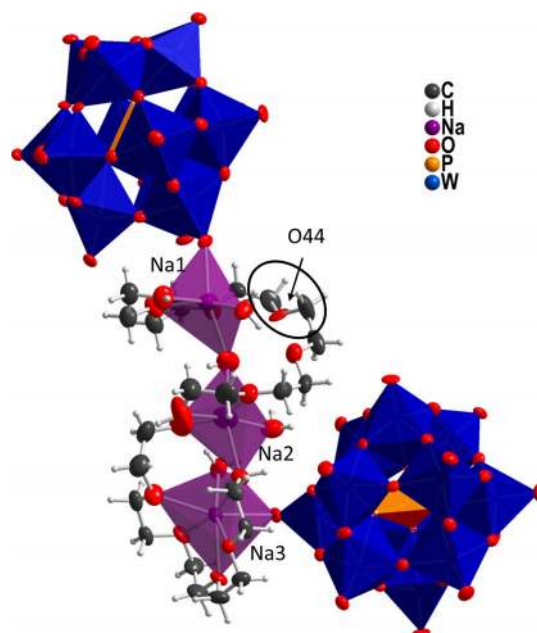

Figure 6. Representation of the coordination polyhedra of Na$^+$ (Na1: distorted octahedron, Na2: distorted octahedron, and Na3: distorted pentagonal bipyramid). The black circle indicates the disordered fragment of the EO$_6$ chain in the crystalline compound due to a long interatomic distance d(O44A–Na1) = 2.77 Å and d(O44B–Na1) = 3.25 Å, respectively. This fragment was refined with split positions; only the major contribution is shown here.

model obtained from single crystal analysis is representative for all crystals (Figure S14).

Surprisingly, two oligomers, one EO$_5$ and one EO$_6$, are embedded in the crystal structure. Hence, salt addition promotes the selective precipitation of EO$_5$–EO$_6$ from an aqueous PEG200 solution, which is composed of a mixture of EO$_x$ oligomers with x ranging from 3–8 (see ESI-MS in the Supporting In-

formation). This implies that EO_x oligomers with $x < 5$ and $x > 6$ remain in the mother liquor. The two oligomers, EO_5 and EO_6, are almost perfectly ordered. Only one -CH_2-O-CH_2 fragment of the EO_6 chain is disordered and had to be refined with split positions in the structure model refinement (not shown in Figure 6 but indicated with a black circle). The EO_6 oligomer forms a nearly full helix around two Na^+ ions. Na1 is fully buried in the EO_6 helix and is in an octahedral coordination of oxygen atoms from a terminal oxygen of PW, two water molecules, and three oxygen atoms of the EO_6 chain. Note, that the disorder of the -CH_2-O-CH_2 fragment may originate from the non-coordinating behavior of O44 to Na1 due to a long interatomic distance d(O44A—Na1) = 2.77 Å and d(O44B—Na1) = 3.25 Å, respectively, for the two positions of O44. Na2 is coordinated by two oxygen atoms stemming from the EO_6 chain, two water molecules, and the terminal -OH functions of the EO_5 chain resulting in a slightly distorted octahedral coordination. Na3 is fully buried in the EO_5 chain, surrounded by a total of seven coordinating oxygen atoms, hence a distorted pentagonal bipyramidal coordination. Note that the EO_5 chain is too short to form a full helix; it has a loop or U-shape conformation.

EO_x chains are well known to adopt a helical conformation in the solid state, which is usually referred to as a 7/2 helix, as seven monomer units form two helical turns.[46,47] Here, EO_6 is long enough to adopt a helical conformation, as found previously in self-assembled monolayers.[48] In the compound under discussion, the presence of sodium in the helical structure produces a larger helix with 6–7 EO units required to form one full helical turn. The value of 3 EO units per sodium cation in the complexes is very common in EO_x-metal alkali complexes, for example with K^+.[49] Here, 9 EO units out of 11 which are available ($EO_5 + EO_6$), are involved in the complexation of the Na^+ cations. Hence, two short EO oligomers are present in the crystal structure in order to provide about 3 EO units per sodium ion. In PEG200, the concentration of EO_9 (or longer EO_x oligomers), which would be long enough to coordinate 3 sodium ions, is negligible. Therefore, it is not observed in the present crystals. For the longer PEGs, PEG300/400, the powder diffractograms indicate the formation of a different crystalline material, which likely contains EO_x oligomers with $x > 6$ (Figure S15 and S16). This is the topic of ongoing investigations. Moreover, PEG300/400 produce smaller crystals as compared to PEG200. This is expected for longer oligomers which have more conformational freedom and therefore prevent the crystal growth.

The helical structure of PEG was previously observed in isobutyric acid/water mixtures, whereas only the coil conformation is formed in pure water.[50]

NMR investigations in water have shown that the internal EO units of EO_x oligomers interact strongly with PW. This implies that the EO_x oligomers adopt a loop or a U-shape conformation in the EO_x–PW nanoassemblies. The internal EO units coordinate towards the PW and the more hydrophilic terminal EO units (-CH_2-CH_2-OH) coordinate towards the water phase. Compared to the nanoassemblies in water (NMR results), no interaction between CH_2 groups and PW can be observed in the

crystal structure, which rather shows a strong complex between Na^+ and O atoms from the PEGs. In the aqueous phase, it is expected that EO_x oligomers adsorbed at the PW surface are still highly flexible and have many degrees of freedom to change their conformations. The addition of NaCl to the nanoassemblies promotes the crystallization. During this process, PEG chains must rearrange, as entropic and enthalpic contributions lead to the coordination of the PEG-oxygens to Na^+ to counterbalance its electron deficiency in the final crystal. Therefore it appears that the nanoassemblies, formed at low concentrations in water, play the role of nuclei for the crystallization process once NaCl (Na^+) is added.

Therefore, the results presented herein strongly suggest that the crystals are in an equilibrium with nanoassemblies spontaneously preformed in water and that the addition of salt (here NaCl) to the PW–EO_x nanoassemblies promotes crystallization of these assemblies by freezing a molecular organization of EO_x chains in the cystal.

Conclusion

It is shown here that the adsorption of POMs on polar surfaces, for example, surfaces covered by EO moieties, is not only due to a surface effect but can be generalized to bulk solutions. Therefore, EO_x oligomers do not have to be located at an interface to promote adsorption of POMs. Scattering techniques (SAXS, SANS) provided a clear evidence of this adsorption in bulk solution whereas NMR clarified the essential role of the internal EO units in the adsorption process. Nanoassemblies consisting of POMs coordinated by loop shaped EO_x oligomers form spontaneously in water by simple mixing of the components. The attraction interactions between PW and EO_x oligomers were found to be stronger by increasing the EO_x length, that is, EO_x with $x > 4$, suggesting that multipolar interactions between internal EO units and POM may be at the origin of the self-assembly process.

The screening of the electrostatic repulsions between EO_x–PW nanoassemblies promotes the formation of a crystalline material. The loop conformation of EO_x at the POM surface seems to act as a nucleus of the EO_x helix/loop conformation found in the crystal. Therefore, EO_x–PW nanoassemblies can be considered as nano building blocks for the formation of POM–hybrid crystalline materials. Moreover, the structure model obtained for PEG200/PW/NaCl crystals indicates that two oligomers with well-defined length, EO_5 and EO_6, are involved per PW. This opens an interesting way for separating oligomers with different polymerization degrees with a high selectively.

The methodology developed here, which is based on the electrostatic screening between pre-formed organic-inorganic EO_x–PW nanoassemblies, can be extended to other kind of water soluble oligomers that interact with POMs in solution. For example the POMs, PW and silicotungstate (SiW), have been found previously to also interact with sugar moieties by adsorbing at surfaces (water-micelle or water-air surfaces) covered by sugar based surfactants.[28] Such a general strategy to build hybrid materials which is based on a self-assembly approach in water has the advantages to avoid the time consum-

ing multi-step synthesis of organic-inorganic POM building blocks as well as the use of toxic polar solvents, such as acetonitrile or DMSO typically employed to dissolve both POMs and organic building blocks. However, the procedure here requires that the POM is chemically stable in water. The rational design of new POM hybrid (crystalline) materials with a simple mixing procedure of the components, as exemplified here with EO_x oligomers and PW, requires a deep understanding of the molecular interactions leading to the formation of the POM-oligomer nanoassemblies.

The very mild synthesis route developed here opens the possibility to build a whole new class of POM composite materials, which may be interesting for their applications in material science, such as ion or proton conducting materials, electrode based materials, photo-responsive hybrid crystals, as well as in catalysis and separation science.

Experimental Section

Materials

Phosphotungstic acid hydrate (PW, $MW = 2898\ g\,mol^{-1}$, $H_3PW_{12}O_{40} \cdot H_2O$, 99.995% purity) was purchased from Sigma Aldrich. The solubility limit of PW in water is above 900 mM, the geometrical diameter of PW is 0.95 nm, providing a volume of $0.54\ nm^3$ per PW. This molecular volume corresponds to a maximum volume fraction of 27% of a concentrated PW solution. TGA measurements revealed that purchased PW contains up to 5 wt.% of water. This was not taken into account for sample preparation. PEG200, PEG300, and PEG400, were purchased from Sigma Aldrich and were of reagent grade. The molecular weights of EO_x with $x = 1$ is $62\ g\,mol^{-1}$ and $44\ g\,mol^{-1}$ more per further repeating $-CH_2-CH_2-O-$ (EO) unit. PEG200 means that the molecular weight average of PEG amounts to $200\ g\,mol^{-1}$, therefore having an average in the size distribution at 4 EO units (PEG300: 6 EO units, PEG400: 8 EO units). This is due to the fact, that PEG polymers consist of mixtures with a distribution on the number of the EO units, for example PEG200 is composed of a mixture of $PEG_{n=3,4,5,6}$ EO units (see Supporting Information). Pure ethylene oxide (EO_1, 99%), diethylene oxide (EO_2, 99%), triethylene oxide (EO_3, 99%), and tetraethylene oxide (EO_4, 99%) were purchased from Sigma Aldrich. In contrast to PEG_x compounds, those chemicals do not exhibit a distribution in their chain length, but have a distinct chain length. Sodium chloride (NaCl, 99.5%) and potassium chloride (KCl, 99%) were purchased from Sigma Aldrich, hydrochloric acid (HCl, 37% for analysis) was purchased from Carlo Erba reagents. Milli-Q water was used with a permittivity lower than $10.5\ \mu S\,cm$ and a total organic carbon content of 400 ppb.

Sample preparation

Crystals were prepared along the same following procedure: an aqueous solution containing EO_x/ PEG_x and salt/acid (HCl, LiCl, NaCl) (solution 1) was cooled down to 4 °C in the refrigerator. A second aqueous solution containing PW and the same amount of salt/acid (solution 2) was also cooled down to 4 °C. Solution 2 was poured gently into solution 1 and left in the refrigerator for 3 days. Then a microscopy analysis was performed to see if crystals were formed or not.

Small angle X-ray scattering (SAXS)

SAXS measurements using Mo radiation ($\lambda = 0.071$ nm) were performed on a bench built by XENOCS. The scattered beam was recorded using a large online scanner detector (diameter: 345 mm, from MAR Research). A large q-range (0.2 to 40 nm^{-1}) was covered with an off-center detection. The collimation was applied using a 12:$\propto$ multilayer Xenocs mirror (for Mo radiation) coupled to two sets of scatterless Forvis slits providing a 0.8×0.8 mm X-ray beam at the sample position. Pre-analysis of data was performed using FIT2D software. The scattered intensities are expressed versus the magnitude of scattering vector $Q = [(4\pi)/\lambda]\sin(\theta/2)$, where λ is the wavelength of incident radiation and θ the scattering angle. 2 mm quartz capillaries were used as sample containers for the solutions. Usual corrections for background subtractions (empty cell and detector noise) and intensity normalization using high density polyethylene film as a standard were applied. Experimental resolution was $\Delta Q/Q = 0.05$. Silver behenate in a sealed capillary was used as the scattering vector calibration standard.

Small angle neutron scattering (SANS)

SANS spectra were recorded at the V16-TOF beamline at the HZB Berlin. The q-range from 0.6 nm^{-1} to 7 nm^{-1} was accessed, which corresponds to sizes from around 0.9 to 10.5 nm in real space. All spectra were corrected for instrumental background and empty cell, and from the incoherent scattering, mainly due to the hydrogen atoms of the PEG_x. The small contribution of PW (constant scattering over the whole q-range) was also subtracted. The scattered intensity was calibrated with water and therefore data are shown in absolute values (cm^{-1}).

Nuclear magnetic resonance (NMR) spectroscopy

All NMR spectra were measured at room temperature using a Bruker Avance 300 (300 MHz for ^1H) NMR spectrometer. All chemical shifts are reported in δ-scale as parts per million [ppm] (multiplicity, coupling constant J, number of protons) relative to the solvent residual peak (D_2O) as the internal standard.

Conflict of interest

The authors declare no conflict of interest.

[1] J. J. Borrás-Almenar, E. Coronado, A. Müller, M. Pope, *Polyoxometalate Molecular Science* Springer Netherlands, **2012**.

[2] S. S. Wang, G. Y. Yang, *Chem. Rev.* **2015**, *115*, 4893 – 4962.

[3] M. V. Vasylyev, R. Neumann, *J. Am. Chem. Soc.* **2004**, *126*, 884 – 890.

[4] A. Dolbecq, E. Dumas, C. R. Mayer, P. Mialane, *Chem. Rev.* **2010**, *110*, 6009 – 6048.

[5] M.-S. Wang, G. Xu, Z.-J. Zhang, G.-C. Guo, *Chem. Commun.* **2010**, *46*, 361 – 376.

[6] R. Prudent, V. Moucadel, B. Laudet, C. Barette, L. Lafanechère, B. Hasenknopf, J. Li, S. Bareyt, E. Lacôte, S. Thorimbert, *Chem. Biol.* **2008**, *15*, 683 – 692.

[7] H. K. Yang, Y. X. Cheng, M. M. Su, Y. Xiao, M. B. Hu, W. Wang, Q. Wang, *Bioorg. Med. Chem. Lett.* **2013**, *23*, 1462 – 1466.

[8] L. Fu, H. Gao, M. Yan, S. Li, X. Li, Z. Dai, S. Liu, *Small* **2015**, *11*, 2938 – 2945.

[9] J. T. Rhule, C. L. Hill, D. A. Judd, R. F. Schinazi, *Chem. Rev.* **1998**, *98*, 327 – 357.

[10] C. Zhang, W. Bu, D. Ni, C. Zuo, C. Cheng, Q. Li, L. Zhang, Z. Wang, J. Shi, *J. Am. Chem. Soc.* **2016**, *138*, 8156 – 8164.

[11] A. Proust, B. Matt, R. Villanneau, G. Guillemot, P. Gouzerh, G. Izzet, *Chem. Soc. Rev.* **2012**, *41*, 7605.

[12] D. L. Long, R. Tsunashima, L. Cronin, *Angew. Chem. Int. Ed.* **2010**, *49*, 1736 – 1758; *Angew. Chem.* **2010**, *122*, 1780 – 1803.

[13] M. Sadakane, E. Steckhan, *Chem. Rev.* **1998**, *98*, 219 – 238.

[14] S. Herrmann, C. Ritchie, C. Streb, *Dalton Trans.* **2015**, *44*, 7092 – 7104.

[15] H. Wang, Y. Yan, B. Li, L. Bi, L. Wu, *Chem. Eur. J.* **2011**, *17*, 4273 – 4282.

[16] L. Leclercq, A. Mouret, A. Proust, V. Schmitt, P. Bauduin, J. M. Aubry, V. Nardello-Rataj, *Chem. Eur. J.* **2012**, *18*, 14352 – 14358.

[17] L. Leclercq, A. Mouret, P. Bauduin, V. Nardello-Rataj, *Langmuir* **2014**, *30*, 5386 – 5393.

[18] G. Izzet, B. Abécassis, D. Brouri, M. Piot, B. Matt, S. A. Serapian, C. Bo, A. Proust, *J. Am. Chem. Soc.* **2016**, *138*, 5093 – 5099.

[19] T. Akutagawa, D. Endo, F. Kudo, S. I. Noro, S. Takeda, L. Cronin, T. Nakamura, *Cryst. Growth Des.* **2008**, *8*, 812 – 816.

[20] Y. Wu, R. Shi, Y. L. Wu, J. M. Holcroft, Z. Liu, M. Frasconi, M. R. Wasielewski, H. Li, J. F. Stoddart, *J. Am. Chem. Soc.* **2015**, *137*, 4111 – 4118.

[21] S. Liu, D. G. Kurth, B. Bredenkötter, D. Volkmer, *J. Am. Chem. Soc.* **2002**, *124*, 12279 – 12287.

[22] S. Liu, D. Volkmer, D. G. Kurth, *J. Cluster Sci.* **2003**, *14*, 405 – 419.

[23] N. Joo, S. Renaudineau, G. Delapierre, G. Bidan, L. M. Chamoreau, R. Thouvenot, P. Gouzerh, A. Proust, *Chem. Eur. J.* **2010**, *16*, 5043 – 5051.

[24] X. Luo, C. Yang, *Phys. Chem. Chem. Phys.* **2011**, *13*, 7892 – 7902.

[25] R. Zhang, C. Yang, *J. Mater. Chem.* **2008**, *18*, 2691.

[26] V. Jallet, G. Guillemot, J. Lai, P. Bauduin, V. Nardello-Rataj, A. Proust, *Chem. Commun.* **2014**, *50*, 6610 – 6612.

[27] S. Landsmann, M. Wessig, M. Schmid, H. Cölfen, S. Polarz, *Angew. Chem. Int. Ed.* **2012**, *51*, 5995 – 5999; *Angew. Chem.* **2012**, *124*, 6097 – 6101.

[28] B. Naskar, O. Diat, V. Nardello-Rataj, P. Bauduin, *J. Phys. Chem. C* **2015**, *119*, 20985 – 20992.

[29] H. Huang, J. Xu, K. Wei, Y. J. Xu, C. K. K. Choi, M. Zhu, L. Bian, *Macromol. Biosci.* **2016**, *16*, 1019 – 1026.

[30] M. W. Tibbitt, K. S. Anseth, *Biotechnol. Bioeng.* **2009**, *103*, 655 – 663.

[31] J. Chen, S. K. Spear, J. G. Huddleston, R. D. Rogers, *Green Chem.* **2005**, *7*, 64 – 82.

[32] S. Zalipsky, J. Harris, *ACS Symp. Ser.* **1997**, *680*, 1 – 13.

[33] S. H. Chung, A. Manthiram, *Adv. Mater.* **2014**, *26*, 7352 – 7357.

[34] *Poly (Ethylene Glycol) Chemistry: Biotechnical and Biomedical Applications* (Ed. J. M. Harris), Springer Science & Business Media, **2013**.

[35] W. Ge, Z. Long, X. Cai, Q. Wang, Y. Zhou, Y. Xu, J. Wang, *RSC Adv.* **2014**, *4*, 45816 – 45822.

[36] J. Tang, W. Yu, M.-B. Hu, Y. Xiao, X.-G. Wang, L.-J. Ren, P. Zheng, W. Zhu, Y. Chen, W. Wang, *ChemPlusChem* **2014**, *79*, 1455 – 1462.

[37] J. Tang, C. Ma, X.-Y. Li, L.-J. Ren, H. Wu, P. Zheng, W. Wang, *Macromolecules* **2015**, *48*, 2723 – 2730.

[38] M. Tsuboi, M. Hibino, N. Mizuno, S. Uchida, *J. Solid State Chem.* **2016**, *234*, 9 – 14.

[39] R. Neumann, M. Lissel, *J. Org. Chem.* **1989**, *54*, 4607 – 4610.

[40] D. Svergun, C. Barberato, M. H. Koch, *J. Appl. Crystallogr.* **1995**, *28*, 768 – 773.

[41] O. F. Erdem, D. Michel, *J. Phys. Chem. B* **2005**, *109*, 12054 – 12061.

[42] J. Wu, Z. Wang, W. Lin, S. Chen, *Acta Biomater.* **2013**, *9*, 6414 – 6420.

[43] J. Mohan, *Organic Spectroscopy: Principles and Applications*, Alpha Science International Limited, **2004**.

[44] R. A. De Graaf, *In Vivo NMR Spectroscopy, 2nd Ed.*, *Principles and Techniques*, Wiley, **2007**.

[45] J. Dust, Z. Fang, J. M. Harris, *Macromolecules* **1990**, *23*, 3742 – 3746.

[46] Y. Takahashi, H. Tadokoro, *Macromolecules* **1973**, *6*, 672 – 675.

[47] R. Yang, X. R. Yang, D. F. Evans, W. A. Hendrickson, J. Baker, *J. Phys. Chem.* **1990**, *94*, 6123 – 6125.

[48] P. Harder, M. Grunze, R. Dahint, G. M. Whitesides, P. E. Laibinis, *J. Phys. Chem. B* **1998**, *102*, 426 – 436.

[49] R. D. Walsh, J. M. Smith, T. W. Hanks, W. T. Pennington, *Cryst. Growth Des.* **2012**, *12*, 2759 – 2768.

[50] M. L. Alessi, A. I. Norman, S. E. Knowlton, D. L. Ho, S. C. Greer, *Macromolecules* **2005**, *38*, 9333 – 9340.